SCIENCE CHINA
Chemistry

• ARTICLES •

October 2015 Vol.58 No.10: 1537–1543
doi: 10.1007/s11426-015-5374-1

Cytotoxicity of mitochondrial-targeting silica-coated manganese oxide nanoparticles

Jie Wei, Chao Yu, Li Wang, Jun Wang, Zhiguo Zhou, Hong Yang* & Shiping Yang

The Key Laboratory of Resource Chemistry of Ministry of Education; Shanghai Key Laboratory of Rare Earth Functional Materials; Shanghai Municipal Education Committee Key Laboratory of Molecular Imaging Probes and Sensors; Shanghai Normal University, Shanghai 200234, China

Received December 29, 2014; accepted January 6, 2015; published online June 1, 2015

The mitochondrion is a promising target for diagnosis and therapy. Mitochondrial-targeting silica-coated manganese oxide nanoparticles ($MnO@SiO_2$-PPh_3^+ NPs) were successfully synthesized to explore the mitochondrial cytotoxicity of nanoparticles. The mitochondrial targeting property was confirmed by a laser scanning confocal microscopy experiment. Even after incubation for only 4 h, the cytotoxicity of $MnO@SiO_2$-PPh_3^+ NPs against cancer cells was obvious; the ATP content was significantly decreased to 40%; and the mitochondrial membrane potential was depleted. All of these results indicated the collapse of mitochondrial function and the start of a cell apoptosis pathway. Our findings suggest that mitochondrial-mediated apoptosis could be strengthened by targeting to the subcellular compartment.

mitochondrial targeting, cytotoxicity, apoptosis, ATP content, mitochondrial membrane potential

1 Introduction

With the rapid development of nanotechnology, many nanoparticles have been related to human life. However, the unexpected side effects of nanotechnology must also be considered. In particular, the toxicity of nanomaterials used for disease diagnosis and therapeutics must be determined. Because so much toxic damage can be caused by nanoparticles, we must consider their toxicity mechanisms.

As we all know, the modified manganese oxide nanomaterials exhibit stupendous potential biological applications for multifunctional imaging and drug delivery [1–4]. Currently, silica-coated manganese oxide nanoparticles ($MnO@SiO_2$ NPs) are considered one of the most important materials for MRI contrast agents that can be loaded with drugs, conjugated with fluorescent dyes or targeted molecules [5–9]. Our group has developed multifunctional silica-coated MnO NPs for targeting MR imaging [10–12]. We also found that $MnO@SiO_2$ NPs can induce mitochondria-mediated apoptosis [13].

The mitochondrion is an important cellular organelle and a significant site of oxidative metabolism. It can not only provide energy for cells but also control programmed cell death. Mitochondria play a significant role in the homeostasis of physiological functions, including electron transfer, apoptosis, cytochrome C release, and calcium storage [14]. The triphenylphosphonium, which consists of a positively charged phosphorus atom surrounded by three hydrophobic phenyl groups, has been utilized for more than 40 years to explore mitochondrial membrane potential as a probe [15–18]. Herein, 2-carboxyethyl-triphenylphosphonium [$COOH$-$(CH_2)_2$-PPh_3^+] was conjugated on the surface of silica-coated MnO NPs to prepare mitochondrial-targeting silica-coated manganese oxide nanoparticles ($MnO@SiO_2$-PPh_3^+ NPs) (Figure 1). The fluorescein dye labeled on the surface of the nanoparticles enabled us to confirm the mitochondrial targeting property with a laser scanning confocal microscopy experiment. Compared with nontargeting $MnO@SiO_2$ NPs, the mitochondrial targeting $MnO@SiO_2$-PPh_3^+ NPs

*Corresponding author (email: yanghong@shnu.edu.cn)

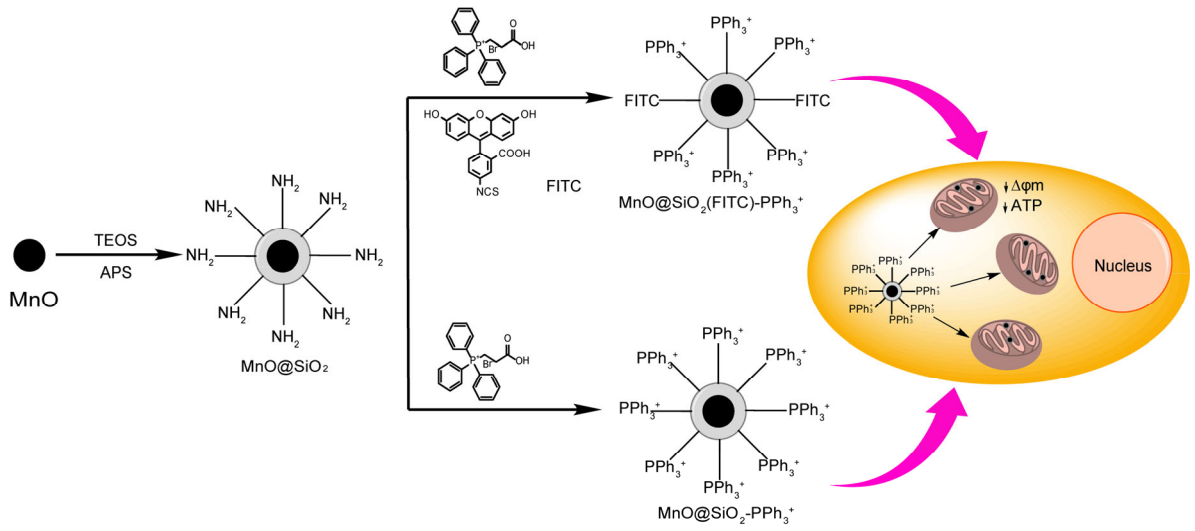

Figure 1 Synthesis route and schematic mitochondrial toxicity of MnO@SiO_2-PPh_3^+ NPs.

exhibited much more obvious toxicity, which resulted in the depletion of ATP content and the depolarization of mitochondrial membrane [19,20].

2 Experimental

2.1 Materials

Manganese chloride tetrahydrate ($MnCl_2 \cdot 4H_2O$) (99.0%), sodium oleate ($C_{18}H_{33}NaO_2$, 90.0%), *n*-octanol ($C_8H_{18}O$, 99.0%), and tetraethylorthosilicate (TEOS) were purchased from Sinopharm Chemical Reagent Co., Ltd. (China); 1-octadecene (90.0%) and 1 g epal CO-520 were purchased from Sigma-Aldrich (USA); aminopropyltriethoxysilane (APS) was purchased from Beijing InnoChem Science & Technology Co, Ltd. (China); *N*-hydroxysuccinimide was purchased from Shanghai Chemical Technology Co, Ltd. (China); 2-carboxyethyl-triphenylphosphonium bromide ($COOH(CH_2)_2$-$PPh_3^+Br^-$) and 1-ethyl-(3-dimethylaminopropyl) carbodiimide hydrochloride (EDC·HCl) were purchased from Accela Chemical Technology (Shanghai) Co., Ltd. (China); fluorescein isothiocyanate (FITC, 1.95%) was purchased from Alfa Aesar Chemical Co. Ltd. (USA); and MitoTracker Red CMXRos were purchased from Qcbic Science & Technologies Co, Ltd. (China). The water used in our experiment was purified through a Milli-Q Plus 185 (USA) with the resistivity of 18 MΩ cm.

2.2 Characterization

X-ray diffraction (XRD) was performed by a Rigaku DMAX 2000 diffractometer (Japan) equipped with Cu-Kα radiation at a scanning rate of 4°/min in the 2θ range of 20°–80° (λ=0.15405 nm, 40 kV, 40 mA). The size and morphology of the nanoparticles were observed by a JEOL JEM-2010 transmission electron microscope (TEM, Japan) operating at 200 kV. The zeta potential and hydrodynamic radius of our nanoparticles were analyzed by a Malvern Zetasizer Nano ZS model ZEN3690 (Worcestershire, UK). UV-Vis spectra were recorded on a spectrophotometer of DU 730 (Beckman Coulter, USA). The fluorescence spectra were determined by a Cary-Eclipse spectrometer (USA). Fluorescence in cells was tested by a flow cytometer (Quanta SC, U.S. Beckman Coulter Company). Fluorescence imaging was conducted by laser scanning confocal microscope (TSC SP5 Ⅱ, Germany Leica Microsystems). Cell viability experiments were recorded on a microplate reader, Multiskan MK3 (Thermo Fisher, USA).

2.3 Preparation of MnO@SiO_2-PPh_3^+ NPs

The aminated silica-coated manganese oxide nanoparticles (MnO@SiO_2 NPs) were synthesized according to our previously published report [13]. To synthesize MnO@SiO_2-PPh_3^+ NPs, three steps were adopted. First, 15 mL anhydrous DMF and 40 mg 2-carboxyethyl-triphenylphosphonium bromide were added to a 100 mL one-neck flask. Second, 50 mg EDC·HCl was added under magnetic stirring at room temperature for 40 min before 100 mg *N*-hydroxysuccinimide was added. Then the solution was stirred for another 40 min. Finally, 15 mL anhydrous DMF that contained 10 mg MnO@SiO_2 NPs was added and the reaction was protected with nitrogen for 24 h. After being washed with ethanol three times, the nanoparticles were stored at 4 °C [21].

2.4 Preparation of fluorescein-labelled silica-coated mitochondrial-targeting MnO nanoparticles (MnO@SiO_2(FITC)-PPh_3^+ NPs)

We added 15 mL anhydrous DMF and 40 mg 2-carboxyethyl-triphenylphosphonium bromide into a single-neck flask

with magnetic stirring. Next, 50 mg EDC·HCl was added under magnetic stirring at room temperature for 40 min before 100 mg *N*-hydroxysuccinimide was added and the mixture was stirred for another 40 min. Next, 10 mg $MnO@SiO_2$ NPs in DMF solution (15 mL) and 5 mg FITC were added to the reaction mixture. Finally, the NPs were protected with nitrogen in dark for 12 h. After being washed with ethanol three times, the nanoparticles were stored at 4 °C.

2.5 Flow cytometric analysis

HeLa cells (human cervical cancer cells) were grown in culture media composed of RPMI-1640 medium supplemented with 10% fetal bovine serum (FBS, gibco, USA), 1% penicillin, and streptomycin at 37 °C in an atmosphere of 5% CO_2 and 95% air. HeLa cells were seeded onto a 6-well plate with the density of 2×10^6 cells/well, and then incubated with $MnO@SiO_2$(FITC)-PPh_3^+ NPs at 0, 25, 50, and 100 μg/mL. The medium was removed after 4 h incubation and the cells were washed twice with cold PBS solution to remove excess nanoparticles. Then the cells were collected by centrifugation after being digested with trypsin. These cells were mixed into 1 mL RPMI-1640 medium and then immediately analyzed by a flow cytometer.

2.6 Laser scanning confocal microscopy experiment

HeLa cells were incubated with 100 μg/mL $MnO@SiO_2$-(FITC)-PPh_3^+ NPs for 4 h, and then incubated with the mitochondrial dye (Mito Tracker RED CMXRos) for another 15 min. Next, these cells were fixed with 4% paraformaldehyde for 20 min. Before these cells were observed on a confocal laser scanning microscope, trypan blue dye was added to quench the fluorescence of the $MnO@SiO_2$-(FITC)-PPh_3^+ NPs and the Mito Tracker RED CMXRos absorbed by the cells. The green and red fluorescence from $MnO@SiO_2$(FITC)-PPh_3^+ NPs and MitoTracker Red CMXRos were excited by 540 and 630 nm, respectively.

2.7 MTT assay

HeLa cells were seeded onto a 96-well plate with the density of 1×10^4 cells/well. $MnO@SiO_2$ NPs, 2-carboxyethyl-triphenylphosphonium bromide and $MnO@SiO_2$-PPh_3^+ NPs with concentrations of 0, 10, 25, 50, 75, and 100 μg/mL were added to a 96-well plate. After incubation for 4 h, 20 μL MTT PBS solution (5 μg/mL) was added to each well. The cells were incubated for another 4 h. Then the upper layer of the solution was discarded and 150 μL DMSO solution was added to each well to dissolve the formazan crystals. The OD value of each well was measured at 490 nm by a microplate reader.

2.8 ATP content test

The ATP content in the HeLa cells was detected with an ATP assay kit (Beyotime, China). The HeLa cells were seeded onto a 6-well plate and incubated for 24 h. After being washed twice with PBS, the medium was removed and 200 μL lysis solution was added to each well; the cells were lysised immediately. Then the cells were centrifuged at 12000 g for 10 min at 4 °C. Afterward, the supernatant solution was tested by a fluorescence spectrophotometer. The ATP content was determined by the standard curve.

2.9 Mitochondrial membrane potential (MMP) test

The change of mitochondrial membrane potential was determined by a mitochondrial membrane potential detection kit (Beyotime, China) on a flow cytometer. A lipophilic dye JC-1 (5,5′,6,6′-tetrachloro-1,1′,3,3′-tetraethylbenzimidazolcarbocyanine iodide) in our detection kit was used. HeLa cells seeded onto the 6-well plate were incubated with nanoparticles at concentrations of of 0, 10, 25, 50, 75, and 100 μg/mL for 4 h. The carbonyl cyanide *m*-chlorophenylhydrazon (CCCP) (10 μmol/L) in the kit was the positive control. The HeLa cells were washed twice with cold PBS and then incubated with JC-1 working solution (5 μg/mL) for 20 min at 37 °C under an atmosphere of 5% CO_2 and 95% air. Then the staining solution was removed and the cells were washed twice with JC-1 working buffer. Last, the cells were resuspended in the 500 μL 1640 culture medium and then analyzed by a flow cytometer. JC-1 in normally polarized mitochondria was aggregated in mitochondrial matrix (J-aggregates) with the red fluorescence; the JC-1 in depolarized mitochondria was in monomer in a mitochondrial matrix with green fluorescence. The red fluorescence resulting from J-aggregates was recorded at E_x/E_m 525/590 nm. The green fluorescence resulting from monomer was recorded at E_x/E_m 490/530 nm.

3 Results and discussion

3.1 Synthesis and characterization

Silica-coated MnO NPs were synthesized according to our previous report [13]. As shown in Figure 2, MnO NPs were 15.6±2.4 nm in diameter. After the conjugation with 2-carboxyethyl-triphenylphosphonium bromide, the silica-coated $MnO@SiO_2$-PPh_3^+ NPs were 46.2±3.6 nm in diameter. The surface potential changed from 25.5 mV for $MnO@SiO_2$ to 37.4 mV for $MnO@SiO_2$-PPh_3^+ NPs. Accordingly, the hydrodynamic radius changed from 91.6 to 94.0 nm. These results suggested that triphenylphosphonium (PPh_3^+) with mitochondria-targeting property was successfully modified on the surfaces of the nanoparticles.

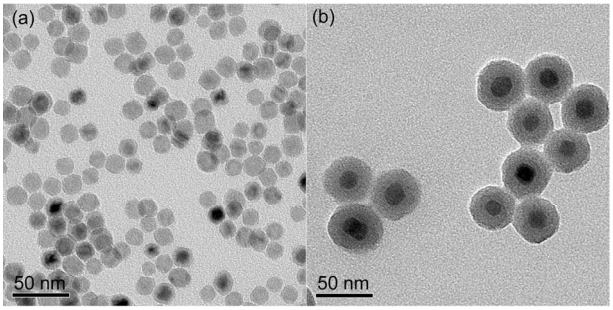

Figure 2 TEM images of MnO NPs (a) and MnO@SiO_2-PPh_3^+ NPs (b).

3.2 Cellular uptake of MnO@SiO_2(FITC)-PPh_3^+ NPs

To investigate the endocytosis of MnO@SiO_2-PPh_3^+ NPs, FITC was conjugated onto the surface of MnO@SiO_2-PPh_3^+ NPs to form MnO@SiO_2(FITC)-PPh_3^+ NPs, which were supported by their strong absorption peaks at 449 and 487 nm, and their maximum emissions at 521 nm (Figure 3(a, b)). To determine the content of the cellular uptake of MnO@SiO_2(FITC)-PPh_3^+ NPs, HeLa cells were incubated with different concentrations of MnO@SiO_2(FITC)-PPh_3^+ NPs for 4 h. As shown in Figure 3, with the increasing concentration of MnO@SiO_2(FITC)-PPh_3^+ NPs, the fluorescence expression level of the HeLa cells was gradually enhanced. The fluorescence expression level reached about 66.8% with the incubation of a maximum concentration of 100 μg/mL. The data from the flow cytometry demonstrated that MnO@SiO_2 (FITC)-PPh_3^+ NPs could be effectively uptaken by the HeLa cells.

3.3 Mitochondria targeting property of MnO@SiO_2-(FITC)-PPh^{3+} NPs

The location of nanoparticles to different cell organelles mainly depends on the type of their modification. In recent years, 2-carboxyethyl-triphenylphosphonium bromide conjugated probes have been used in numerous studies that focused on mitochondria associated responses [22]. To further assess the sub-cellular compartmentalization of MnO@SiO_2(FITC)-PPh_3^+ NPs, we co-stained HeLa cells with NPs and MitoTracker Red CMXRos. As shown in the confocal laser experiments depicted in Figure 4(b), the uptake of MnO@SiO_2(FITC)-PPh_3^+ NPs by HeLa cells could be effectively confirmed. The merged luminescent images (Figure 4(d)) of MnO@SiO_2(FITC)-PPh_3^+ NPs and MitoTracker Red CMXRos probes showed good correspondence, which indicated high specificity to mitochondria.

3.4 The cytotoxicity of MnO@SiO_2-PPh_3^+ NPs in HeLa cells

The cytotoxicity of MnO@SiO_2 NPs, 2-carboxyethyltriphenylphosphonium bromide ($COOH(CH_2)_2$-$PPh_3^+Br^-$) and MnO@SiO_2-PPh_3^+ NPs were further evaluated by a standard MTT assay. The cell viability of MnO@SiO_2 NPs and

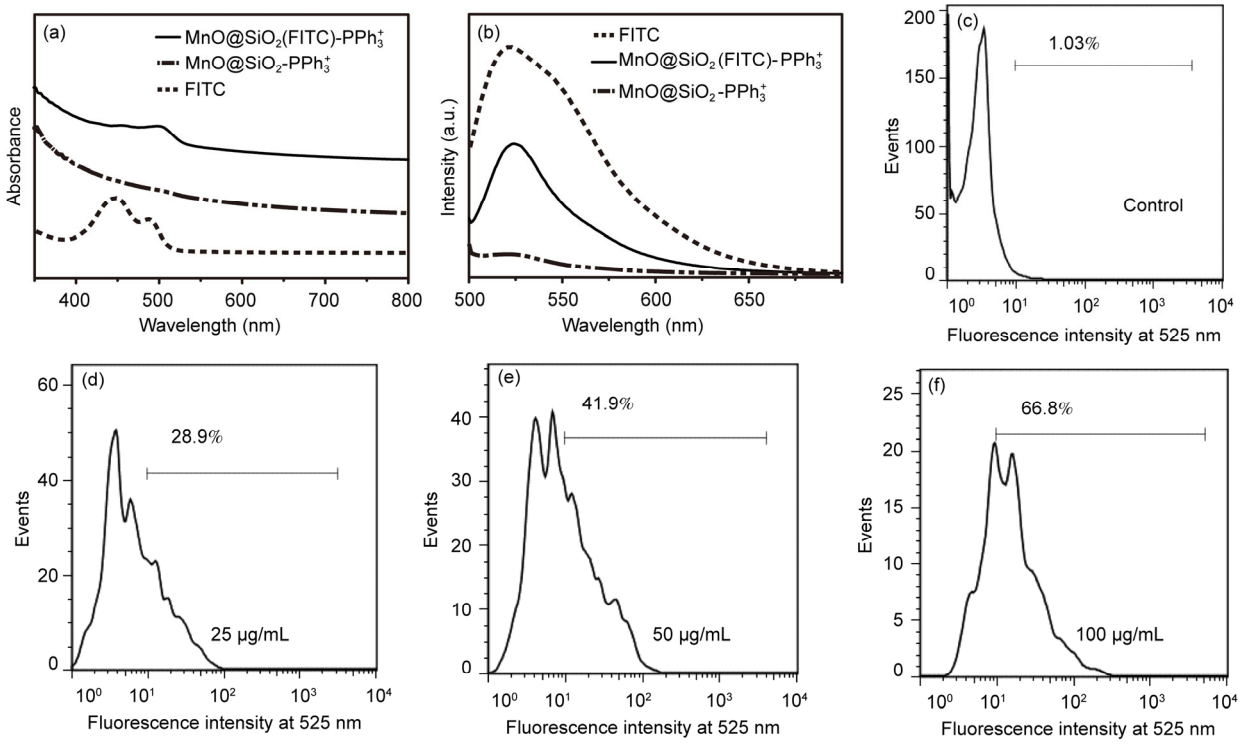

Figure 3 The UV-Vis absorption (a) and fluorescence (b) spectra of MnO@SiO_2(FITC)-PPh_3^+ NPs, MnO@SiO_2-PPh_3^+ NPs, and FITC. Flow cytometry profiles of HeLa cells treated with MnO@SiO_2(FITC)-PPh_3^+ NPs with the concentration of 0 (c), 25 (d), 50 (e), and 100 μg/mL (f).

$COOH(CH_2)_2$-$PPh_3^+Br^-$ were all above 90% after incubation for 4 h, but the cell viability of MnO@SiO_2-PPh_3^+ NPs induced greater cytotoxicity and exhibited a concentration-dependent cytotoxicity. These results were in line with our previous report [13], which showed that the toxicity of MnO@SiO_2NPs was highly time-dependent. However, the viability decreased significantly after 8 h. In strong contrast, the cell viability of HeLa cells was sharply decreased with the increasing concentration of MnO@SiO_2-PPh_3^+ NPs and reached 57% with the concentration of 100 μg/mL after incubation for 4 h (Figure 5). The mitochondria-targeting MnO@SiO_2-PPh_3^+ NPs showed cytotoxicity even at the concentration of 10 μg/mL. The IC50 value was 50 μg/mL. These results indicated that MnO@SiO_2-PPh_3^+ NPs caused the death of cancer cells within 4 h. All of these results suggested that the mitochondria-targeting property can effectively improve the cytotoxicity of nanoparticles.

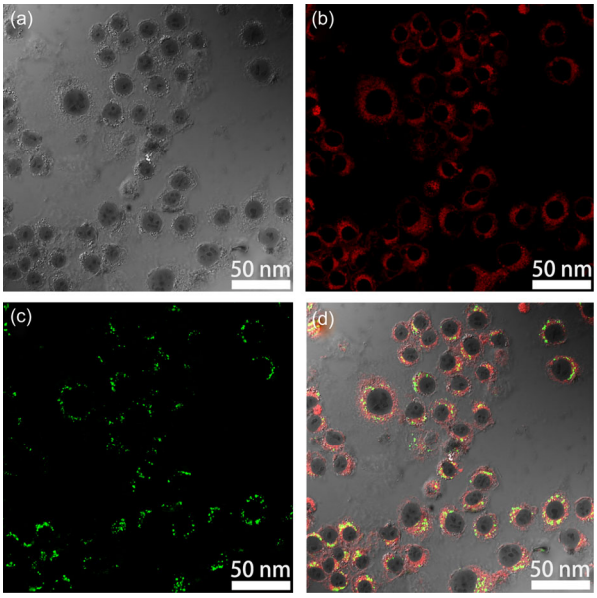

Figure 4 (a) Confocal images of HeLa cells of the bright field; (b) the fluorescence image after incubation of MnO@SiO_2(FITC)-PPh_3^+ NPs; (c) the fluorescence image after incubation of MitoTracker Red CMXRos; (d) the merged image of (b) and (c).

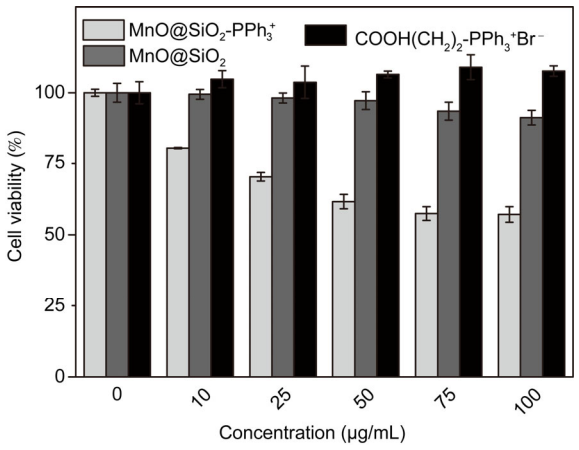

Figure 5 Cell viability of HeLa cells incubated with MnO@SiO_2-PPh_3^+ NPs, MnO@SiO_2 NPs, and $COOH(CH_2)_2$-$PPh_3^+Br^-$.

3.5 Mitochondrial toxicity of MnO@SiO_2-PPh_3^+ NPs in HeLa cells

As we all know, a change in mitochondrial membrane potential is a sign of cell apoptosis. To further illustrate the effects of nanoparticles on the mitochondria, the loss of mitochondrial membrane potential (MMP) was measured. Generally, JC-1 dye is an indicator of mitochondrial activity to detect the change of the mitochondrial membrane potential (MMP). Although JC-1 was aggregated in the normal mitochondrial matrix with the red fluorescence, it only existed in the cytoplasm as a monomer with the green fluorescence. Therefore, the change of the proportion of red/green fluorescence can directly reflect the transformation of MMP [23–25]. As presented in Figure 6, almost all MMP of HeLa cells incubated with different concentrations of MnO@SiO_2-PPh_3^+ NPs showed different levels of loss in a concentration-dependent way. For example, the red/green fluorescence ratio with the concentration of 10–100 μg/mL

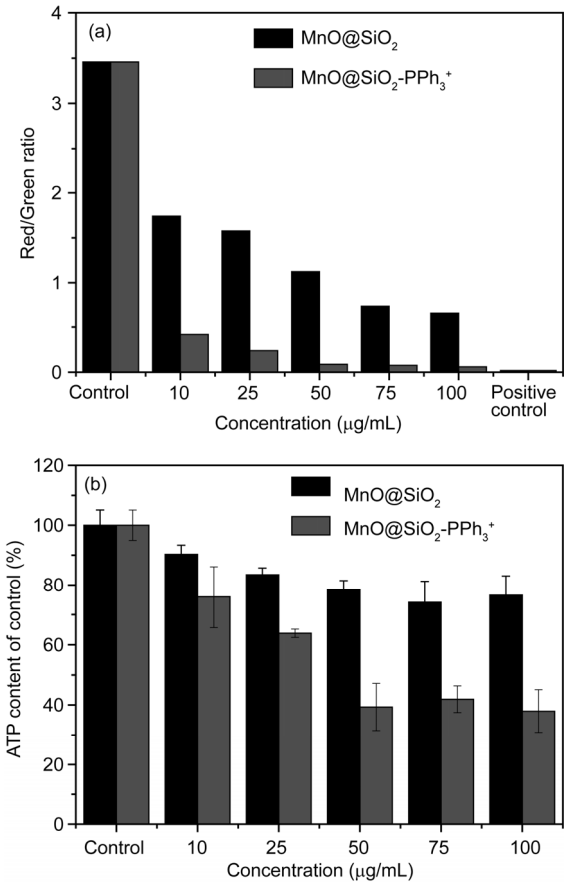

Figure 6 Changes of MMP (a) and ATP content (b) for HeLa cells incubated with different concentrations of MnO@SiO_2 and MnO@SiO_2-PPh_3^+ NPs.

decreased almost sevenfold. The significant decrease of MMP began to emerge at the concentration of 50 μg/mL and the impact subsequently declined to 100 μg/mL. The mitochondrial membrane potential of $MnO@SiO_2$-PPh_3^+ NPs was almost completely depleted at the concentration of 100 μg/mL. Furthermore, the downward trend of MMP after the incubation of $MnO@SiO_2$-PPh_3^+ NPs was much more than that of $MnO@SiO_2$ NPs, which demonstrated that the mitochondrial membrane had truly been damaged.

Mitochondria, which are significantly important to metabolism, supply almost all of the ATP to the cells and are also involved in both apoptotic and necrotic cell death. Because the considerable consumption of ATP can seriously affect the metabolism of cells [26–28], the depletion of ATP was further determined. After incubation with $MnO@SiO_2$-PPh_3^+ NPs for 4 h, significant depletion of ATP was observed in the HeLa cells. The content of ATP decreased significantly with concentrations of 0–50 μg/mL, by approximately 60%. However, the rate declined gradually from the concentration of 50–100 μg/mL, where there was a steady decline. The highest amount of ATP depletion (63%) was generated after the HeLa cells were exposed to 100 μg/mL $MnO@SiO_2$-PPh_3^+ NPs for 4 h. All of the data suggested that the $MnO@SiO_2$-PPh_3^+ NPs produced more significant levels of ATP and mitochondrial membrane potential depletion than those of $MnO@SiO_2$ NPs, which proved the superiority of mitochondria-targeting inhibitory effect from another aspect.

4 Conclusions

We designed $MnO@SiO_2$-PPh_3^+ NPs to demonstrate their mitochondria-targeting ability and to induce the severe damage to cancer cells. The $MnO@SiO_2$ NPs exhibited noncytotoxicity in about 4 h and the mitochondria-targeting $MnO@SiO_2$-PPh_3^+ NPs induced severe cytotoxicity in the same period. Most importantly, the mitochondria-targeting property facilitated cell death. The cytotoxicity of $MnO@SiO_2$-PPh_3^+ NPs resulted from the cell action of mitochondrial damage, including the depletion of ATP content and the dissipation of mitochondrial membrane potential. This method can be extended to the field of medical therapy.

This work was supported by the National Natural Science Foundation of China (21271130, 21371122), the Program for Changjiang Scholars and Innovative Research Team in University (IRT1269), the Shanghai Science and Technology Development Fund (12ZR1421800, 13520502800), the Shanghai Pujiang Program (13PJ1406600), the Shanghai Municipal Education Commission (13ZZ110), Shanghai Normal University (SK201339), and the International Joint Laboratory on Resource Chemistry.

1 Chen Y, Yin Q, Ji X, Zhang S, Chen H, Zheng Y, Sun Y, Qu H, Wang Z, Li Y, Wang X, Zhang K, Zhang L, Shi J. Manganese oxide-based multifunctionalized mesoporous silica nanoparticles for pH-responsive MRI, ultrasonography and circumvention of MDR in cancer cells. *Biomaterials*, 2012, 33: 7126–7137
2 Chen Y, Chen H, Zhang S, Chen F, Sun S, He Q, Ma M, Wang X, Wu H, Zhang L, Shi J. Structure-property relationships in manganese oxide-mesoporous silica nanoparticles used for T1-weighted MRI and simultaneous anti-cancer drug delivery. *Biomaterials*, 2012, 33: 2388–2398
3 Shin J, Anisur RM, Ko MK, Im GH, Lee JH, Lee IS. Hollow manganese oxide nanoparticles as multifunctional agents for magnetic resonance imaging and drug delivery. *Angew Chem Int Ed*, 2009, 48: 321–324
4 Na HB, Lee JH, An K, Park YI, Park M, Lee IS, Nam DH, Kim ST, Kim SH, Kim SW, Lim KH, Kim KS, Kim SO, Hyeon T. Development of a T1 contrast agent for magnetic resonance imaging using MnO nanoparticles. *Angew Chem Int Ed*, 2007, 46: 5397–5401
5 Patricia C, Patricia de la P, Pilar M, Marta M, José María A, Guillermo R, Félix Y, José María GC, Antonio H. Magnetism in nanoparticles: tuning properties with coatings. *J Phys-Condens Mat*, 2013, 25: 484006
6 Kim T, Momin E, Choi J, Yuan K, Zaidi H, Kim J, Park M, Lee N, McMahon MT, Quinones-Hinojosa A, Bulte JWM, Hyeon T, Gilad AA. Mesoporous silica-coated hollow manganese oxide nanoparticles as positive T_1 contrast agents for labeling and MRI tracking of adipose-derived mesenchymal stem cells. *J Am Chem Soc*, 2011, 133: 2955–2961
7 Schick I, Lorenz S, Gehrig D, Schilmann AM, Bauer H, Panthöfer M, Fischer K, Strand D, Laquai F, Tremel W. Multifunctional two-photon active silica-coated Au@MnO Janus particles for selective dual functionalization and imaging. *J Am Chem Soc*, 2014, 136: 2473–2483
8 Sahoo B, Devi KSP, Dutta S, Maiti TK, Pramanik P, Dhara D. Biocom patible mesoporous silica-coated superparamagnetic manganese ferrite nanoparticles for targeted drug delivery and MR imaging applications. *J Colloid Interf Sci*, 2014, 431: 31–41
9 Zhan QQ, Qian J, Li X, He SL. A study of mesoporous silica-encapsulated gold nanorods as enhanced light scattering probes for cancer cell imaging. *Nanotechnology*, 2010, 21: 055704
10 Hu H, Dai A, Sun J, Li X, Gao F, Wu L, Fang Y, Yang H, An L, Wu H, Yang S. Aptamer-conjugated $Mn_3O_4@SiO_2$ core-shell nanoprobes for targeted magnetic resonance imaging. *Nanoscale*, 2013, 5: 10447–10454
11 Yang X, Zhou Z, Wang L, Tang C, Yang H, Yang S. Folate conjugated $Mn_3O_4@SiO_2$ nanoparticles for targeted magnetic resonance imaging *in vivo*. *Mater Res Bull*, 2014, 57: 97–102
12 Yang H, Zhuang Y, Hu H, Du X, Zhang C, Shi X, Wu H, Yang S. Silica-coated manganese oxide nanoparticles as a platform for targeted magnetic resonance and fluorescence imaging of cancer cells. *Adv Funct Mater*, 2010, 20: 1733–1741
13 Yu C, Zhou Z, Wang J, Sun J, Liu W, Sun Y, Kong B, Yang H, Yang S. In depth analysis of apoptosis induced by silica coated manganese oxide nanoparticles *in vitro*. *J Hazard Mater*, 2015, 283: 519–528
14 Smith RA, Hartley RC, Murphy MP. Mitochondria-targeted small molecule therapeutics and probes. *Antioxid Redox Sign*, 2011, 15: 3021–3038
15 Ross MF, Kelso GF, Blaikie FH, James AM, Cochemé HM, Filipovska A, Da Ros T, Hurd TR, Smith RAJ, Murphy MP. Lipophilic triphenylphosphonium cations as tools in mitochondrial bioenergetics and free radical biology. *Biochemistry*, 2005, 70: 222–230
16 Liberman EA, Topaly VP, Tsofina LM, Jasaitis AA, Skulachev VP. Mechanism of coupling of oxidative phosphorylation and the membrane potential of mitochondria. *Nature*, 1969, 222: 1076–1078
17 Murphy MP, Smith RAJ. Targeting antioxidants to mitochondria by conjugation to lipophilic cations. *Annu Rev Pharmacol*, 2007, 47: 629–656
18 Rokitskaya TI, Sumbatyan NV, Tashlitsky VN, Korshunova GA, An

tonenko YN, Skulachev VP. Mitochondria-targeted penetrating cations as carriers of hydrophobic anions through lipid membranes. *Biochim Biophys Acta*, 2010, 1798: 1698–1706
19 Pang CC, Sun WJ, Xiao D, Ding L, Bu HF. Novel *2H*-pyrazolo-[4,3-c]hexahydropyridine derivatives: synthesis, crystal structure, fluorescence properties and cytotoxicity evaluation against human breast cancer cells. *Sci China Chem*, 2013, 56: 702–715
20 Zhang CN, Wang W, Wang CH, Tian Q, Hang W, Yuan Z, Chen XS. Cytotoxicity of liver targeted drug-loaded alginate nanoparticles. *Sci China Chem*, 2009, 52: 1382–1387
21 Du W, Xu X, Zhang D, Lu Q, Gao F. Green synthesis of MnO_x nanostructures and studies of their supercapacitor performance. *Sci China Chem*, 2015, 58: 1–7
22 Park SY, Oh KT, Oh YT, Oh NM, Youn YS, Lee ES. An artificial photosensitizer drug network for mitochondria-selective photodynamic therapy. *Chem Commun*, 2012, 48: 2522–2524
23 Reers M, Smiley ST, Mottola-Hartshorn C, Chen A, Lin M, Chen LB. Mitochondrial membrane potential monitored by JC-1 dye. *Methods Enzymol*, 1995, 260: 406–417
24 Perelman A, Wachtel C, Cohen M, Haupt S, Shapiro H, Tzur A. JC-1: alternative excitation wavelengths facilitate mitochondrial membrane potential cytometry. *Cell Death Dis*, 2012, 3: e430
25 Lemasters JJ, Nieminen AL, Qian T, Trost LC, Elmore SP, Nishimura Y, Crowe RA, Cascio WE, Bradham CA, Brenner DA, Herman B. The mitochondrial permeability transition in cell death: a common mechanism in necrosis, apoptosis and autophagy. *Biochim Biophys Acta*, 1998, 1366: 177–196
26 Murphy MP, Smith RAJ. Drug delivery to mitochondria: the key to mitochondrial medicine. *Adv Drug Deliver Rev*, 2000, 41: 235–250
27 Yaffe MP. The Machinery of mitochondrial inheritance and behavior. *Science*, 1999, 283: 1493–1497
28 Nishikawa T, Edelstein D, Du XL, Yamagishi S, Matsumura T, Kaneda Y, Yorek MA, Beebe D, Oates PJ, Hammes HP, Giardino I, Brownlee M. Normalizing mitochondrial superoxide production blocks three pathways of hyperglycaemic damage. *Nature*, 2000, 404: 787–790